

pubs.acs.org/JPCC Article

# Dissolution Amplification by Resonance and Cavitational Stimulation at Ultrasonic and Megasonic Frequencies

Ross A. Arnold, Shiqi Dong, Longwen Tang, Dale Prentice, Marie Collin, Juan Carlos Vega-Vila, Amaya Hernandez, Erika Callagon La Plante, Kirk Ellison, Aditya Kumar, Samanvaya Srivastava, Mathieu Bauchy,\* Dante Simonetti,\* and Gaurav N. Sant\*



Cite This: J. Phys. Chem. C 2022, 126, 3432-3442

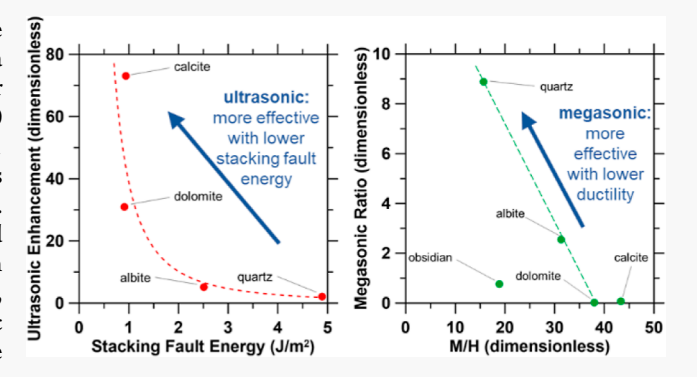


ACCESS I

Metrics & More

Article Recommendations

ABSTRACT: Acoustic stimulation offers a green pathway for the extraction of valuable elements such as Si, Ca, and Mg via solubilization of minerals and industrial waste materials. Prior studies have focused on the use of ultrasonic frequencies (20–40 kHz) to stimulate dissolution, but megasonic frequencies (≥1 MHz) offer benefits such as matching of the resonance frequencies of solute particles and an increased frequency of cavitation events. Here, based on dissolution tests of a series of minerals, it is found that dissolution under resonance conditions produced dissolution enhancements between 4x-to-6x in Si-rich materials (obsidian, albite, and quartz). Cavitational collapse induced by ultrasonic stimulation was more effective for Ca- and Mg-rich carbonate precursors (calcite and dolomite), exhibiting a significant increase



in the dissolution rate as the particle size was reduced (i.e. available surface area was increased), resulting in up to a 70× increase in the dissolution rate of calcite when compared to unstimulated dissolution for particles with  $d_{50}$  < 100  $\mu$ m. Cavitational collapse induced by megasonic stimulation caused a greater dissolution enhancement than ultrasonic stimulation (1.5× vs 1.3×) for amorphous class F fly ash, despite its higher Si content because the hollow particle structure was susceptible to breakage by the rapid and high number of lower-energy megasonic cavitation events. These results are consistent with the cavitational collapse energy following a normal distribution of energy release, with more cavitation events possessing sufficient energy to break Ca-O and Mg-O bonds than Si-O bonds, the latter of which has a bond energy approximately double the others. The effectiveness of ultrasonic dissolution enhancement increased exponentially with decreasing stacking fault energy (i.e., resistance to the creation of surface faults such as pits and dislocations), while, in turn, the effectiveness of megasonic dissolution increased linearly with the stacking fault energy. These results give new insights into the use of acoustic frequency selections for accelerating elemental release from solutes by the use of acoustic perturbation.

# INTRODUCTION

Sonication has been proposed as an efficient pathway to facilitate dissolution of sparingly soluble minerals and industrial wastes, thereby liberating desirable species such as Ca, <sup>1-3</sup> Mg, <sup>3-6</sup> K, <sup>7-9</sup> Na, 9 Al, 3,10 Si, 2,5,11 and Ni 12 for the sustainable manufacture of mineral products. The cavitation induced by acoustic stimulation promotes extraction of elements from the solute by concentrating energy at the particle surface, resulting in localized temperature increases by up to 5000 K and pressure increases up to 1000 bar. 13 This enhanced dissolution occurs in the absence of strong acids or bases and thus, leads to an environmentally benign process. 14

When subjected to an acoustic field, cavitation bubbles undergo rapid expansion and contraction cycles, leading to an increase in overall bubble size until the bubbles reach a critical (i.e., resonance) size, at which the bubbles collapse. 15 The rapid (<1  $\mu$ s), near-adiabatic<sup>16</sup> collapse of these bubbles causes the aforementioned localized hot spots of energy. Several criteria can influence cavitation behavior, including system temperature, particle size, particle composition, and the acoustic stimulation frequency. <sup>17–19</sup> The focus of this study is the comparative effects of two stimulation frequencies: 20 kHz (ultrasonic) and 1 MHz (megasonic). Ultrasonically enhanced dissolution of minerals has focused on stimulation at low ultrasonic frequencies (i.e., 16-40 kHz). 1,2,4,20-22 In contrast, megasonic stimulation (i.e.,

December 31, 2021 Received: Revised: January 27, 2022 Published: February 9, 2022





greater than 1 MHz) is used for fine tasks such as the cleaning of delicate equipment (e.g., microchips,  $^{23-27}$  flat panel displays, photomasks, or etc.). These varied stimulation frequencies give rise to different critical cavitation bubble sizes, with values of  $\sim 150~\mu m$  at 20 kHz and of  $\sim 4~\mu m$  at 1 MHz. Thus, the cavitation-induced dissolution enhancement is different at the different frequencies.

Larger bubbles produce more energy per cavitational collapse, as the energy released by a cavitation bubble is proportional to the square of the radius of the collapsing bubble, <sup>32</sup> allowing for the breakage of higher-energy bonds. Higher-frequency acoustic stimulation reduces the likelihood of cavitation events (i.e., cavitational collapse), 16 with a negligible occurrence of cavitational events due to the high applied pressure (>1 MPa) required to form cavitation bubbles when stimulated at acoustic frequencies greater than a few MHz. 33-35 This limits the application of megasonic cavitation to values below ~3 MHz. 16 The cavitation bubble propagation-growth-collapse cycle, however, occurs much more rapidly for megasonic stimulation for two reasons: (1) megasonic critical bubble diameter is nearly 2 orders of magnitude smaller than ultrasonic critical bubble diameter, and the time required for cavitation bubbles to reach their critical radius is approximately proportional to the square of the radius; <sup>32</sup> and (2) the Bjerknes forces (i.e., attractive forces within a sonic field which cause bubbles to coalesce 36,37) are proportional to the square of the stimulation frequency.<sup>38</sup> Thus, though the energy per cavitational collapse is much greater at ultrasonic frequencies, the rate of occurrence of cavitational collapse is much more rapid at megasonic frequencies.

Stimulation at megasonic frequencies also allows for matching of the resonance frequency of the solute; that is, the stimulation frequency which causes a particle to oscillate at a much higher amplitude than at any other stimulation frequency. Rapid vibration of the solute particles leads to particle fracture, which releases elemental species into solution more rapidly than unstimulated dissolution from the solute surface. In this study, the study of resonance frequency is limited to intraparticle vibrations at a specific composition and particle size; interparticle resonance frequencies for particles assembled in a single solid are possible, but due to the irregularity in shape and composition of natural rocks, this possibility is not studied herein.

The structure and composition of the solute determine the extent to which the frequency of acoustic stimulation affects dissolution rates. The energy required to induce dissolution often increases with increasing bond energy and with increasing crystallinity. For this study, calcite (a crystalline Ca-rich mineral), dolomite (crystalline and Ca- and Mg-rich), obsidian (amorphous and Si-rich), and albite and quartz (crystalline and Si-rich) were dissolved under stirred, ultrasonically stimulated, and megasonically stimulated conditions, with macroscopic temperature and agitation rate kept constant between the three conditions. In this way, the effectiveness of ultrasonic and megasonic stimulation frequencies was tested for solutes with varying elemental composition and crystallinity. In addition, molecular dynamics simulations allowed for assessment of the resonance frequency of each solute as a function of particle size, which informed the manner in which the dissolution rate of each solute should be assessed when stimulated at its intraparticle resonance frequency. These results offered a reference basis to dissolution rates which were then compared to the dissolution rates with a particle size an order of magnitude greater and lower than the particle size which corresponded to resonance. It

should be noted here that the Si-O bond energy is more than double that of Ca-O or Mg-O (799.6  $\pm$  13.4, 383.3  $\pm$  5.0, and  $358.2 \pm 7.2$  kJ/mol, respectively<sup>39</sup>). However, rather than the bond energy alone, the stacking fault energy (i.e., the energy required for the formation of a fault such as a dislocation or pit) allows for a more quantitative estimate of the effects on dissolution of different types of acoustic stimulations. 40,41 Materials with a greater resistance to dislocations (i.e., possessing a higher stacking fault energy) are less sensitive to defect formation by cavitational collapse, 40,42,43 and thus, resonance stimulation offers an alternative method for using acoustic energy to enhance dissolution rates when fault formation is unfavorable. Against these considerations, it is shown that ultrasonic stimulation was more effective with the increasing Ca content and lower stacking fault energy, while megasonic stimulation when matched to the resonance particle size was more effective for enhancing the dissolution of Si-rich

#### MATERIALS AND METHODS

**Materials.** Five mineral species (all from VWR, Radnor, PA) were studied: obsidian (81% SiO<sub>2</sub>, 9% Al<sub>2</sub>O<sub>3</sub>, 5% K<sub>2</sub>O, 5% Na<sub>2</sub>O), calcite (CaCO<sub>3</sub>), dolomite (CaMg[CO<sub>3</sub>]<sub>2</sub>), albite (NaAlSi<sub>3</sub>O<sub>8</sub>), and quartz (SiO<sub>2</sub>). The obsidian was completely amorphous, whereas the other four species were crystalline. Minerals were crushed by hand and then separated into three different particle sizes using sieves: (1) <0.1 mm, (2) a particle size such that the resonance frequency corresponded to 1 MHz, and (3) ~1 cm. Resonance frequencies of 20 kHz corresponded to particle sizes greater than 20 cm, whereas an ultrasonic horn only produces cavitation over a distance of ~5 cm, <sup>44</sup> and thus, particles sized to possess a resonance frequency of 20 kHz could not be dissolved. In addition to the minerals, a class F (i.e., Capoor) fly ash (FA) was selected as an amorphous alkaline industrial waste comprised of hollow amorphous aluminosilicate spheres, as a contrast with the non-hollow mineral species. The FA was washed for 50 min at room temperature in DI water with a solid-to-liquid ratio (s/l) of 1:1000 to remove all readily soluble components. After washing, the class F FA was determined to be ~2.2 wt % CaO, significantly lower than the SiO<sub>2</sub> (50.7 wt %), Al<sub>2</sub>O<sub>3</sub> (23.4 wt %), and Fe<sub>2</sub>O<sub>3</sub> (16.7 wt %) contents. The sum of all other oxide components of the FA represented less than 3 wt %. The FA particle size was <30  $\mu$ m and thus could not be tested at the resonance frequency, as it was determined to be in the order of 100-1000 MHz, that is, ultrahigh frequency, which is primarily used for medical imaging<sup>45</sup> as it does not cause disintegration of the exposed solids.

Resonance Frequency. Resonance frequency of the materials was determined via molecular dynamics (MD) simulations, making use of the open-source LAMMPS package. As a non-crystalline phase, obsidian was simulated using a random stoichiometrically correct atomic distribution which was melted at 4000 K for 1 ns, cooled to 300 K under zero pressure in 3.7 ns, and then relaxed at 300 K for 1 ns. Calcite, dolomite, albite, and quartz structures were constructed based on crystallographic data (sources shown in Table 1) and relaxed at 300 K for 500 ps under zero pressure. In all cases, Coulombic, short-range bonded, and van der Waals interactions were considered in calculating the potential energy of the system, with the latter interaction estimated using the CLAYFF or Buckingham potential, as listed in Table 1. The temperature was controlled using a Nosé—Hoover thermostat, 47,48 and the

**Table 1. Mineral Properties for Resonance Frequency Determination** 

mineral	structure reference	forcefield	particle size with resonance frequency of 1 MHz (mm)
obsidian	glassy (non-crystalline)	Buckingham <sup>50</sup>	2.0
calcite	51	Buckingham <sup>52</sup>	2.0
dolomite	53	Buckingham <sup>52</sup>	3.9
albite	54	CLAYFF <sup>55</sup>	3.9
quartz	56	Buckingham <sup>57</sup>	3.5

timestep was taken as 1 fs. To determine the resonance frequency, the stiffness tensor was determined based on the average stress computed from 12 independent deformations (i.e., 3 normal and 3 shear deformations, each being repeated both for a positive and negative strain) by applying a strain of 0.0005. The bulk modulus was taken as the arithmetic mean of the Voigt and Reuss bulk moduli. The simulated values of the density and bulk modulus were then used to determine the resonance frequency, assuming homogeneity, isotropicity, and sphericity of each particle. Torsional resonance frequency values were chosen for this work, since they correspond to the fundamental resonance frequency. The torsional resonance frequency,  $f_{\text{torsional}}$ , was calculated according to eq 1 mentioned below

$$f_{\text{torsional}} = \frac{k_{\text{L}} \sqrt{\frac{K}{\rho}}}{2\pi R} \tag{1}$$

In eq 1,  $k_{\rm L}$  represents a solution to the characteristic equation of torsional oscillations (eq 2), K is the bulk modulus,  $\rho$  is the density, and R is the radius of the presumed spherical particles. The characteristic equation of torsional oscillations is

$$(n-1)j_n(k_L) - k_L j_{n+1}(k_L) = 0; \qquad n \ge 0$$
 (2)

In eq 2, n is an integer  $\geq 0$ , and  $j_n(k_L)$  is the Bessel function of order n. The n=0 solutions in eq 2 were used because they gave the lowest resonance frequency values.

Resonance frequencies of 20 kHz were found to occur for particle sizes >200 mm, several orders of magnitude too large for a practical dissolution experiment. The resonance frequency values and the corresponding references are shown in Table 1.

**Stacking Fault Energy.** Stacking fault energy was assessed for the four crystalline mineral species studied: calcite, dolomite, albite, and quartz. The stacking fault energy characterizes the energy barrier which serves as an obstacle to the activation of a stacking fault defect, such as a dislocation. By this definition, stacking fault energy could not be assessed for amorphous species. A detailed explanation of the stacking fault energy calculation is described elsewhere. In all cases, the slip plane which possessed the lowest stacking fault energy value was chosen as the slip plane of interest for this study.

Dissolution Experiments. 1 g of solute was placed in 100 mL of deionized water (18  $M\Omega$ ·cm) in a 250 mL beaker. This solid-to-liquid ratio (s/l) of 1:100 allowed for a balance of having sufficient solubilized solid to be detectable, while remaining at far-from-equilibrium dissolution concentrations regardless of the particle sizes studied. Ultrasonic dissolution was performed at 20 kHz stimulation using a 505 Sonic Dismembrator ultrasonic horn (Fisher Scientific, Waltham, MA). Megasonic dissolution was performed at 1 MHz stimulation using a Series 6000 HyperClean Megasonic System

(PCT Systems Inc., San Jose, CA). A control ("stirred") experiment was performed using a magnetic stir bar to convectively mix the system. The stir bar rotation speed was set at 350 rpm, as this matched the Reynolds number (Re) of 3900 of the ultrasonically stimulated experiments.<sup>2,59</sup> The megasonic tank did not introduce agitation, so an overhead stirrer was used to obtain a match Re-value. Dissolution rates obtained from the control experiments showed similar experimental error whether the magnetic stir bar or the overhead stirrer was used. Experiments were performed isothermally (at a macroscopic level) at  $40.0 \pm 1.0$  °C. For the stirred and 20 kHz experiments, temperature was maintained using a jacketed beaker. For the 1 MHz dissolution, the temperature was maintained using an integrated temperature control bath and verified by using a thermocouple. In this way, all experiments were performed with the same macroscopic temperature and convective mixing rate, allowing for isolation of the effects of the acoustic perturbation (cavitation and/or resonance vibration).

To determine elemental release rates, 1.0 mL solvent samples were taken at prescribed time intervals. Samples were passed through 0.2  $\mu$ m filters to remove undissolved solids. These samples were diluted 1:1 for obsidian and quartz and 1:3 for calcite, dolomite, albite, and FA (volume basis) with 5% HNO<sub>3</sub> and then analyzed using an Avio 200 inductively coupled plasma optical emission spectrometer (PerkinElmer, Waltham, MA). The concentration of dissolved Si, Ca, or Mg in each sample was determined by comparison to calibration standards prepared by dilution from 1000  $\mu$ g/L standards (Inorganic Ventures, Christiansburg, VA). The apparent dissolution rate constant was determined from a straight-line plot of the concentration of the target element versus the square root of time, referred to in the literature as the "parabolic model",  $^{60-63}$  as follows: [M] = k·  $t^{0.5}$ , where, [M] represents the concentration of element M (Si for obsidian, albite, quartz, and class F FA; Ca for calcite; and Mg for dolomite), k is the apparent parabolic rate constant, and t is time. This model has been found to be applicable in cases where the coprecipitation of elemental species from the bulk solution may affect the overall dissolution kinetics. 62 Although the systems were analyzed at far-from-equilibrium concentrations, co-precipitation reactions affected the apparent rates of dissolution since far-from-equilibrium concentrations of elements such as Si, Al, and Ca are still sufficient to cause minor coprecipitation. The parabolic model is an empirical fit. Although there is no physical meaning to the square root of time, parabolic kinetics have been observed to hold for up to 1 week of dissolution.11

Obsidian, calcite, and class F FA particles of the smallest particle size fraction were collected after dissolution, filtered through 11  $\mu$ m filter paper (Whatman Filter 1, Cytiva, Marlborough, MA) under vacuum, and then dried overnight at 50 °C. Undissolved particles and dried particles after dissolution experiments were characterized using scanning electron microscopy (SEM, Phenom ProX G2, Nanoscience Instruments, Phoenix, AZ) to assess surface changes, visually, following dissolution. The same particles were tested using N<sub>2</sub> adsorption to assess surface area (Anton Paar, Torrance, CA) which indicated that (i) the particle porosity was low [initial Brunauer–Emmett–Teller (BET) surface area <1 m²/g for all samples], and (ii) the change in porosity following dissolution was minimal (change in the BET surface of <10% for all samples following all dissolution techniques).

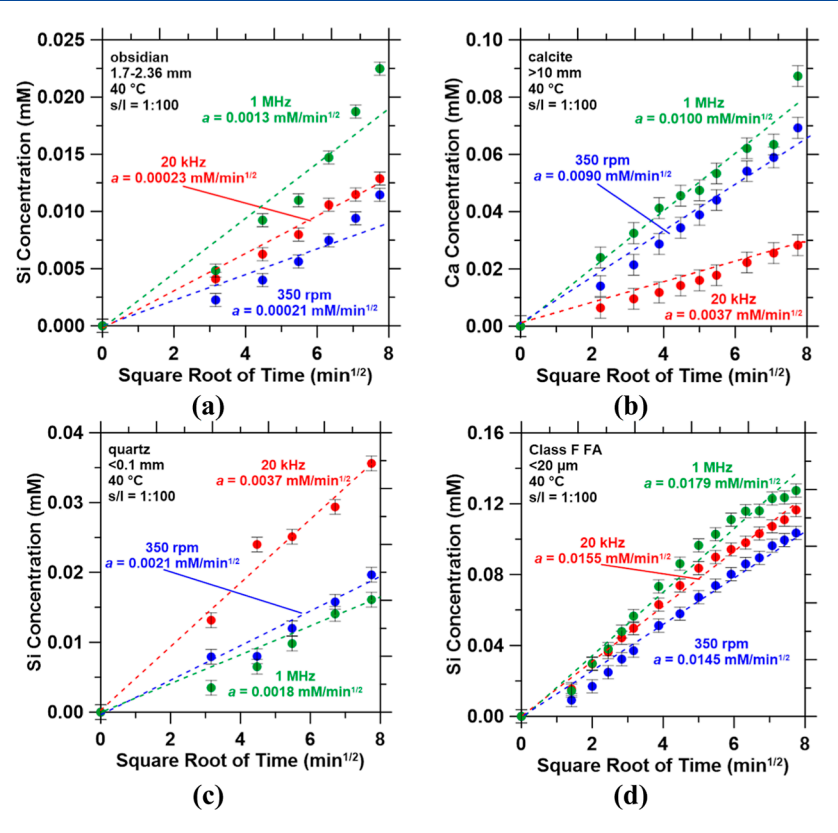
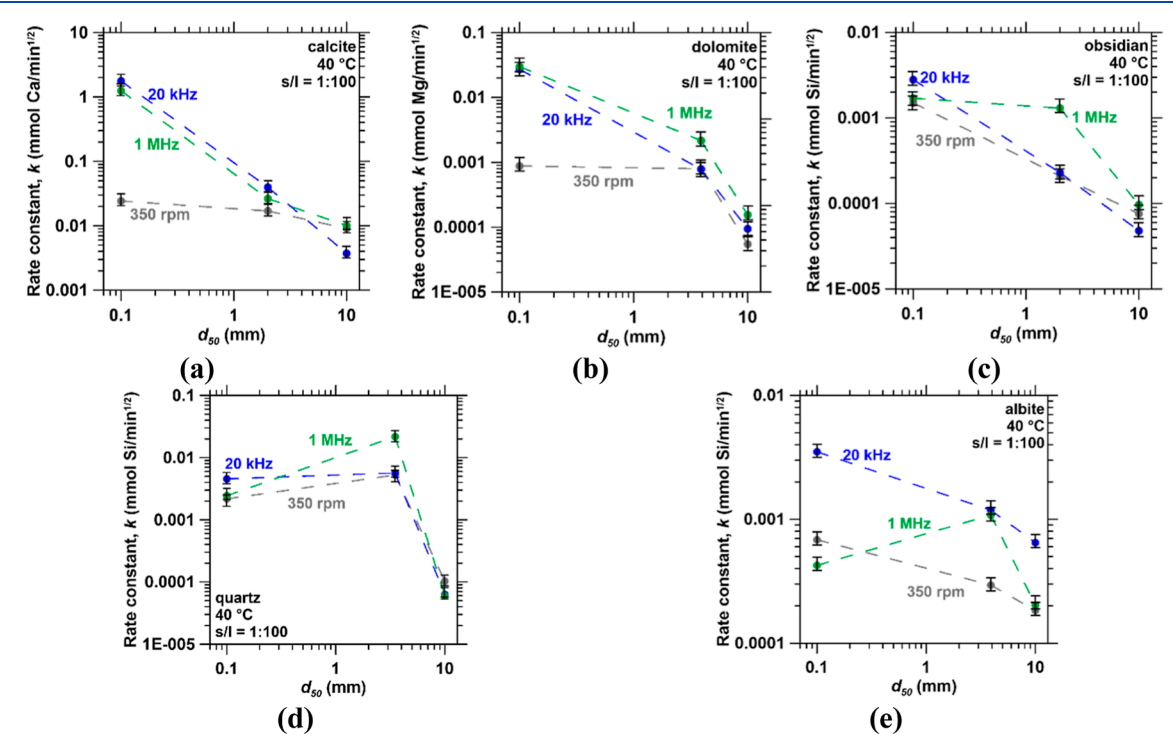


Figure 1. Representative data showing Si concentrations as a function of the square root of time with parabolic dissolution kinetics rate constants indicated for (a) obsidian at the resonance particle size; (b) calcite at the largest particle size; (c) quartz at the smallest particle size; and (d) class F FA at the as-received particle size. Error bars indicate a variability of less than 5% relative standard deviation across all samples.



**Figure 2.** Median particle size vs apparent parabolic rate constant of stirred, ultrasonicated, and megasonicated dissolution for (a) calcite, (b) dolomite, (c) obsidian, (d) quartz, and (e) albite. In all cases, a resonance frequency of 1 MHz corresponds to the middle particle size tested. Error bars indicate a variability of less than 5% in relative standard deviation from triplicate samples.

#### RESULTS AND DISCUSSION

Parabolic Dissolution Kinetics. Parabolic kinetics were used to represent the dissolution of all six species studied (i.e., five minerals and class F FA). Each mineral species was tested at three particle sizes: (1) a particle size where the resonance frequency corresponded to 1 MHz (2-4 mm, depending on the species; see Table 1), (2) a particle size around 1 order of magnitude larger (1 cm), and (3) a particle size an order of magnitude smaller (<0.1 mm). Class F FA could only be tested at the as-received particle size of  $<30 \mu m$ . There were 48 dissolution curves collected in total: three dissolution conditions (stirred, ultrasonically stimulated, and megasonically stimulated) for five mineral species each at three particle sizes and class F FA. All curves followed parabolic kinetics; as an example, the three dissolution conditions for four of these species (obsidian, calcite, quartz, and class F FA) at varying particle sizes are shown in Figure 1. The fit was least accurate for the slowdissolving species (quartz, Figure 1c, and especially obsidian, Figure 1b), where initial kinetics were linear, meaning the parabolic model overestimated the initial rate of dissolution. The dissolution kinetics were well-fitted by the parabolic model which included surface effects, boundary layer effects, and coprecipitation effects, 60-62 which all lead to deviations from linear dissolution kinetics. As the experiments were performed at s/l = 1:100 (i.e., far-from-equilibrium or undersaturated conditions), the influence of coprecipitation reactions was expected to be minimal. The parabolic fits revealed rate constants varying from  $2 \times 10^{-4}$  mM/min (obsidian, 350 rpm, Figure 1a) to 0.018 mM/min (class F FA, 1 MHz, Figure 1d), a range of 2 orders of magnitude demonstrating the suitability of the parabolic model for first-hour dissolution kinetics of both relatively slow- and fast-dissolving species.

Cavitational Dissolution Enhancement. Acoustic perturbation produces cavitation bubbles which collapse to create localized spots at high temperature (5000 K) and high pressure (1000 bar).<sup>64</sup> The effect of this cavitational collapse on the dissolution rate is observed in Figure 2. As expected, a decrease in particle size led to an increase in the overall dissolution rate; however, the efficacy of reducing particle size to increase the dissolution rate depended on the solute studied. The alkalineearth-rich species [calcite (Figure 2a) and dolomite (Figure 2b)] showed the strongest dependence between particle size and dissolution enhancement by acoustic stimulation. For each of these two species, the increase in the dissolution rate by acoustic stimulation was negligible at a particle size of 1 cm, no more than double at the middle particle size, and up to 70× at the smallest particle size (<0.1 mm). For the Si-rich species [obsidian (Figure 2c), quartz (Figure 2d), and albite (Figure 2e)], the rate enhancement by ultrasonication (20 kHz) reached a maximum of 10-fold at the smallest particle size. For both quartz and albite (Figure 2d,e), megasonic (1 MHz) stimulation showed a higher Si release rate at the resonance particle size than at the smallest particle size. Megasonic stimulation was most effective for increasing the dissolution rate at the smallest particle size for Caand Mg-rich solutes and was most effective at the resonance particle size for Si-rich solutes. Ultrasonic stimulation was the most effective at the smallest particle size for all mineral species.

For cavitational collapse to cause dissolution enhancement, the collapse must impart sufficient energy to break solute bonds, and the collapse must occur at the solute—solvent interface. Reducing the particle size increases the available surface area because the porosity of the precursors was low (BET surface

area  $< 1 \text{ m}^2/\text{g}$ ). Increasing available surface area and, in turn, increasing the probability of cavitation occurring at the solutesolvent interface induce the release of target species into solution. The energy released by cavitational collapse at a fixed acoustic frequency follows a normal distribution. 40 Cavitation events which cause bond breakage must possess sufficient energy to rupture the bond. Reducing solute particle size (or increasing solid loading, etc.) leads to higher dissolution rates by providing an increased surface area on which cavitation events may take place, maximizing the likelihood of favorable cavitation. Although an increased surface area increases the unstimulated dissolution rate due to an increase in solid-liquid interfacial area, the effectiveness of cavitation is further enhanced as the proportion of reaction-favorable cavitation events is increased in addition to the active dissolution area. However, dissolution enhancement is closely related to bond energy. Compositionally, of the elements studied, the Si-O bond energy is the highest  $(799.6 \pm 13.4 \text{ kJ/mol})^{39}$  followed by the Ca–O  $(383.3 \pm 5.0 \text{ kJ/mol})^{39}$  and then Mg–O  $(358.2 \pm 7.2)$ kJ/mol) bond energy.<sup>39</sup> Based on these results in Figure 2, the effectiveness of acoustic stimulation to induce dissolution increases with decreasing bond energy between the element of interest and an oxygen atom. The difference between the cavitation behaviors for the different acoustic frequencies is due to both the difference in size of the propagated bubbles and the difference in the frequency of bubble propagation. Cavitation energy increases proportionally with the increasing bubble radius<sup>32</sup> and is thus 37.5× higher for ultrasonic stimulation than megasonic stimulation.<sup>16</sup> Conversely, the bubble propagation growth-collapse cycle is much more rapid for megasonic stimulation, as the rapidity of this cycle is proportional to acoustic frequency<sup>38</sup> and inversely proportional to the bubble radius.<sup>32</sup> Increasing the acoustic frequency from 20 kHz to 1 MHz results in a 50× increase in frequency and a 37.5× reduction in critical bubble size, suggesting an increase in the cavitation bubble cycle by a factor of  $\sim$ 1875.

Megasonic and ultrasonic stimulation demonstrates similar Mg release rates from dolomite (Figure 2d). Mg-O has the lowest bond energy, and thus, the higher energy of ultrasonic cavitation events and the higher rate of megasonic cavitation events provide comparable dissolution rate enhancements. Solutes with lower bond energies than that of Mg-O would be expected to show higher dissolution enhancement by megasonic stimulation than by ultrasonic stimulation, even at small particle sizes. The ultrasonic enhancement of calcite dissolution is higher than that of megasonic enhancement (Figure 2a) because ultrasonic cavitational collapse provides a greater number of cavitation events with sufficient energy to break the Ca-O bonds in calcite. As previously estimated, the frequency of cavitation events is ~1875 greater in megasonic dissolution than in ultrasonic dissolution. Accordingly, the lower enhancement by megasonic dissolution (1.4× lower) implies that the majority of megasonic cavitation events do not possess sufficient energy to break Ca-O bonds. The dissolution enhancement values for Si-rich minerals at the smallest particle size were lower than 10-fold for ultrasonication and were approximately 1 (i.e., no enhancement) for megasonication (Figure 2c-e). These low enhancement values suggest that the majority of ultrasonic cavitation events do not possess sufficient energy to induce Si-O bond breakage, and none of the megasonic cavitation events possess sufficient energy to rupture Si-O bonds.

Resonance Dissolution Enhancement. In addition to inducing cavitation in the solvent, acoustic stimulation causes the solute particles to oscillate at the rate of the stimulation (i.e., 20 kHz or 1 MHz). The middle particle sizes chosen for each of the species in Figure 2 represent the particle size for which the resonance frequency was 1 MHz. For alkaline-earth-rich calcite and dolomite (Figure 2a,b), cavitation caused significant dissolution enhancement, rendering the further dissolution enhancement by resonance stimulation negligible. For the Sirich species (obsidian, quartz, and albite), in contrast, the dissolution enhancement by resonance stimulation (i.e., megasonic stimulation at the particle size corresponding to a resonance frequency of 1 MHz) was  $4-6\times$  (Figure 2c-e). Thus, rapid oscillation at the resonance frequency causes a significant increase in the dissolution rate for minerals with high bond energies, such as Si-rich species. As no particle fracture or surface defect creation of Si-rich species such as quartz under acoustic stimulation has been observed in the literature, <sup>40</sup> the increased dissolution rate is likely due to increased solute-solvent interaction offered at high oscillations, which would result in a near-negligible reduction in particle size. This has been observed in slight changes of the surface morphology from crystalline species exposed to ultrasonic stimulation.<sup>65</sup>,

For albite (Figure 2e), the resonance dissolution rate was greater than the stirred dissolution rate at the smallest particle size tested (1.6× greater), though it was only one-third of that observed for ultrasonication at the smallest particle size. For quartz (Figure 2d), the resonance dissolution rate was greater than even the ultrasonicated dissolution rate at the smallest particle size (4.8× greater) and was similarly 4.8× greater than the highest rate observed for stirred dissolution. This study found a twofold increase in the quartz dissolution rate by ultrasonication due to the reduced particle size (literature studies finding that no rate enhancement was performed with flat polished surfaces of the minerals<sup>2,40</sup>), which greatly increased the available surface area that could be affected by cavitation events with sufficient energy to affect and enhance dissolution processes. This suggests that the reduction in particle size is more effective for increasing the cavitational dissolution rate than for increasing the unstimulated dissolution rate. Overall, as the Si content increased, the influence of oscillation at the resonance frequency on the dissolution rate increased, as other dissolution enhancement pathways (particle fracture, fault formation, etc.) became irrelevant.

Structural Dissolution Enhancement. The five mineral species studied were all of a similar macroscopic structure, being comprised of rigid, non-hollow, and irregularly shaped (i.e., at a macroscopic scale) particles. For comparison, a washed Ca-poor class F FA was also tested to assess the effect of acoustic stimulation on the Si release rate (Figure 3). The washing removed the readily soluble components of the FA, allowing for quantification of the dissolution of the aluminosilicate hollow spheres which remained. As shown in Figure 3, despite the Sirich nature of the FA, megasonic stimulation still produced a 1.5× increase in the Si release rate constant. This increase was not due to resonance stimulation, since the FA particle size was less than 30  $\mu$ m. The increase was also not due to the bond energies, as the composition was primarily Si and Al; Al-O bond energy is  $501.9 \pm 10.6 \text{ kJ/mol}$ , much greater than that of Mg-O or Ca-O. Rather, the enhancement was due to the hollow macroscopic structure of the particles comprising the FA. SEM images of obsidian, calcite, and class F FA before and after dissolution are shown in Figure 4. Obsidian is shown as an

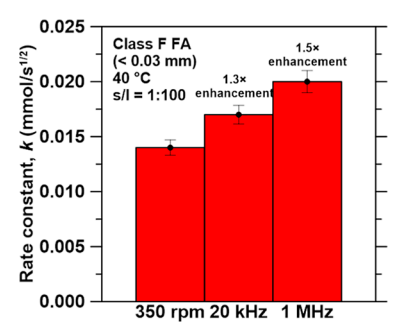


**Figure 3.** Representative parabolic Si release rate constant under stirred, ultrasonically stimulated, and megasonically stimulated dissolution of class F FA. Error bars indicate a variability of less than 5% in relative standard deviation from triplicate samples.

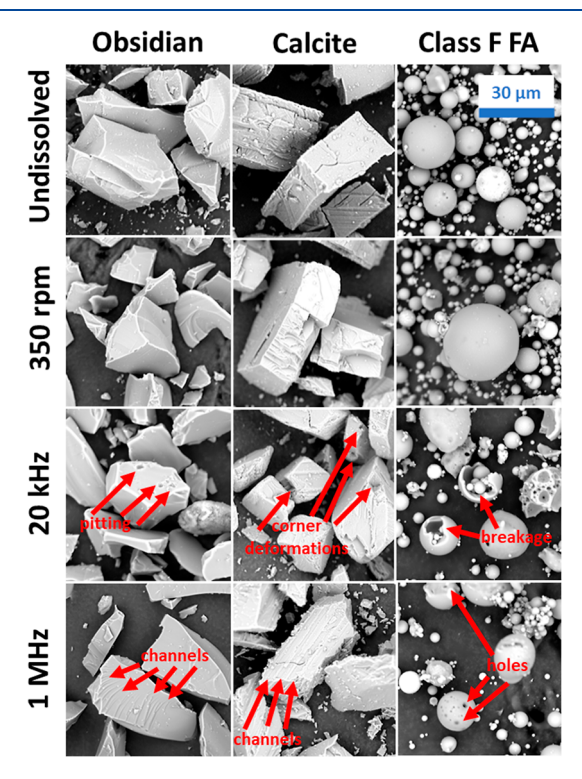


**Figure 4.** Representative SEM images of obsidian, calcite, and class F FA (particle size < 0.1 mm) prior to and after dissolution under stirred (350 rpm), ultrasonically stimulated (20 kHz), and megasonically stimulated (1 MHz) conditions. Cavitation effects (i.e., pits, channels, deformations, breakages, and holes) are emphasized by red arrows and text. The scale bar in top right applies to all images shown.

amorphous Si-rich material similar to class F FA, whereas calcite is shown as a representative of the solutes with compositions with lower bond energies due to the low Si content. For all three materials, no noticeable difference (at the micron scale) was observed between the raw material and the solute after dissolution under convectively mixed conditions; the dissolution incurred by stirring did not alter the micron-scale structural appearance of any of the materials. Ultrasonically dissolved calcite shows significant rounding of the edges and corners of the crystals. The larger ( $\sim 150~\mu m$ ) bubbles induced by ultrasonic cavitation caused breakages at crystal edges, facilitating edge erosion and inducing particle fracture, as observed previously. Some surface pitting is observed in obsidian after ultrasonic stimulation, while the dulling of particle edges is less prominent than for calcite. No pitting was observed in the calcite surface,

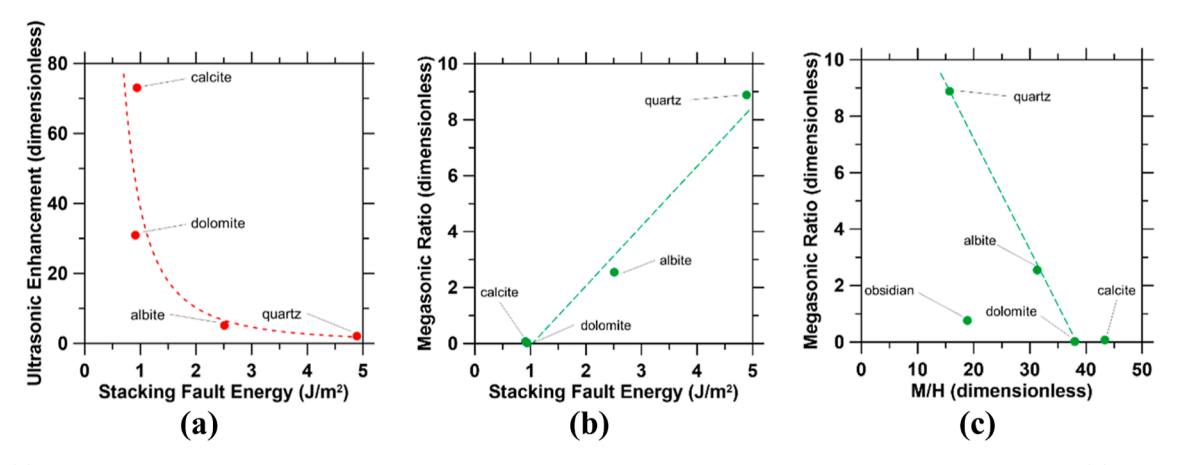


Figure 5. (a) Ultrasonic enhancement for  $d_{50} \sim 0.1$  mm for calcite, dolomite, quartz, and albite as related to stacking fault energy. (b) Megasonic ratio for calcite, dolomite, quartz, and albite as related to the stacking fault energy. (c) Megasonic ratio for calcite, dolomite, quartz, albite, and obsidian as related to the brittleness ratio ( $M_I/H$ ;  $M_I$  = indentation modulus, H = hardness) of the solute.

demonstrating that any pitting caused in the calcite surface led to subsequent particle breakage and/or erosion, and thus, no prominent pits are seen.

Megasonic dissolution of both obsidian and calcite shows evidence of erosion channels not observed after ultrasonic or stirred dissolution. The smaller ( $\sim$ 4  $\mu$ m) bubbles created by megasonic stimulation likely caused shallower pits on the surface of the solute which were not observable under 2000× magnification, and these pits provided areas which were more prone to dissolution, facilitating the creation of channels over the course of the dissolution period, with these channels observable in the SEM images. The channels were much more prominent in the calcite, concurring with the much greater dissolution rate of calcite (Figure 2a) compared to obsidian (Figure 2c). Though obsidian is amorphous and calcite is crystalline, both materials are comprised of particles free of hollow cavities. The hollow spheres of the class F FA, conversely, were observed to be broken after acoustic stimulation. Under ultrasonic stimulation, the aluminosilicate spheres demonstrated holes which were greater than 3  $\mu$ m in diameter, with some spheres broken in half. Ultrasonically induced cavitational collapse was sufficient to rupture the hollow FA particles, even though results with solid (i.e., not hollow) Si-rich minerals (Figure 2c-e) suggested that the majority of ultrasonic cavitation was insufficient to break Si-O bonds. Megasonic stimulation did not show complete particle breakage, but several openings of  $<1 \mu m$  were visible on the particle surfaces. The pitting and fracture induced by megasonic stimulation in FA particles led to dissolution enhancement (Figure 3). In addition to breaking atomic bonds and rapidly oscillating solute particles, cavitation collapse also causes defects in the micron-scale structure of hollow particle, such that an increased defect density gives rise to enhanced solute dissolution rates.

**Acoustic Dissolution Enhancement and Material Properties.** An earlier study<sup>40</sup> compared the dissolution enhancement by ultrasonic stimulation to two intrinsic physical properties of the solute: (i) the stacking fault energy (i.e., the energy required for the formation of faults such as dislocations or pits) and (ii) the surface energy (i.e., the energy required to induce fracture in a material). The stacking fault energy, in particular, allows for quantification of the effects observed in Figure 2, in that both the ultrasonic and megasonic dissolution enhancement can be correlated to the stacking fault energy (Figure 5a,b). The dissolution enhancement effect of ultrasonic

stimulation was estimated using the ratio between the apparent parabolic rate constant under ultrasonic and stirred conditions, each at the smallest particle size

ultrasonic enhancement = 
$$\frac{k_{20\text{kHz,0.1mm}}}{k_{350\text{rpm,0.1mm}}}$$
(3)

The behavior of megasonic stimulation at the resonance and smallest particle sizes, conversely, was estimated using the ratio between the two apparent parabolic rate constants

megasonic ratio = 
$$\frac{k_{1\text{MHz,resonance}}}{k_{1\text{MHz,0.1mm}}}$$
(4)

The curves in Figure 5a,b demonstrate that the effectiveness of both ultrasonic and megasonic dissolution is a function of the stacking fault energy. Materials with lower stacking fault energy are more susceptible to defect formation by cavitational collapse, and thus, ultrasonication is more effective. Materials with higher stacking fault energy are more resistant to defect formation. An increased stacking fault energy indicates materials which are less ductile<sup>67–70</sup> (or more brittle) and thus are most susceptible to dissolution by particle fracture (i.e., rather than stacking fault initiation), which is facilitated by the rapid vibration of stimulation at the resonance frequency. This is further validated by the inverse linear correlation between the megasonic ratio and indentation modulus-to-hardness (M<sub>I</sub>/H) ratio in Figure 5c, the latter of which serves as a proxy for the ductility of a material (since the  $M_{\rm I}/H$  ratio corresponds to the inverse of a yield strain). Note that here, the indentation modulus was calculated based on the simulated stiffness using data from the MD simulations,<sup>74</sup> while hardness was obtained from microindentation tests in the literature.<sup>2</sup> The correlation between ultrasonic enhancement and stacking fault energy (Figure 5a) shows two asymptotes. First, as the stacking fault energy approaches zero, the enhancement approaches an infinite value. The asymptotic approach to infinite enhancement as stacking fault energy approaches zero represents immediate and complete collapse under any cavitation of the structure of the materials with no resistance to dislocation formation. As the stacking fault energy increases, the dissolution enhancement ratio approaches a value of one (i.e., no enhancement in the dissolution rate from acoustic stimulation). A material with an extremely high stacking fault energy, and hence an extremely high resistance to dislocation formation, would be completely

unaffected by cavitational collapse at the surface. Acoustic stimulation is unable to cause surface defects in such a case, leading to identical dissolution behavior as in the unstimulated, convectively mixed system.

The megasonic dissolution ratio increases linearly with the stacking fault energy (Figure 5b). As the resistance to stacking fault formation increases, the dependency of the dissolution rate on particle fracture increases (i.e., since sonication cannot initiate any stacking faults), and thus, the rapid particle vibration at the resonance frequency has a stronger effect on increasing the dissolution rate. The x-intercept of Figure 5b occurs at a stacking fault energy of approximately 1 J/m<sup>2</sup>. Below this value, the sensitivity to resonance stimulation is negligible as the sensitivity to cavitational collapse is much greater. The stacking fault energy of 1 J/m<sup>2</sup> may represent a threshold value for megasonic cavitation at a frequency of 1 MHz: for solutes with a stacking fault energy less than  $1 \text{ J/m}^2$ , megasonic cavitation is sufficiently energetic to serve as the dominant means of dissolution enhancement. For solutes with a greater stacking fault energy than 1 J/m<sup>2</sup>, resonance vibration affects the dissolution rate alongside cavitational enhancement, with the resonance effect increasing as the stacking fault energy increases. Furthermore, resonance dissolution enhancement increases with brittleness (i.e., reduced ductility), as shown in Figure 5c. Highly brittle quartz is the most susceptible to resonance, while dolomite and calcite demonstrate double the M<sub>I</sub>/H ductility of quartz and thus are negligibly susceptible to resonance dissolution enhancement. The lone exception to the trend in Figure 5c is obsidian, which is due to its amorphous nature, leading to a different dissolution enhancement mechanism—not currently clear—from the crystalline solutes studied. The x-intercept of Figure 5c occurs at  $M_I/H \sim 38$ , suggesting this as the ductility threshold, above which the ductility of the material is too high for the dissolution rate to be affected by resonance vibration. Brittle materials demonstrate a tendency to fracture when oscillated rapidly at the resonance frequency, while ductile materials are relatively unaffected by the rapid vibration offered by resonance frequency. In brief, cavitational dissolution enhancement is optimal for precursors susceptible to fracture and fault formation, while resonance dissolution enhancement is preferred for brittle materials.

# SUMMARY AND CONCLUSIONS

Acoustic stimulation can accelerate solute dissolution via two processes: rapid oscillation of particles at the applied acoustic frequency and generation of cavitation bubbles which create localized hot spots of increased temperatures and pressures, facilitating liberation of atomic species from the solute framework. Cavitational collapse is most effective for solutes with lower average bond energies and for those with lower stacking fault energies. Cavitation-induced dissolution enhancement increases with reduced particle size (i.e., increased available surface area), up to a factor of 70× for calcite. Ultrasonic stimulation, which produces larger cavitation bubbles (150  $\mu$ m at 20 kHz), and megasonic stimulation, which produces smaller cavitation bubbles (4  $\mu$ m at 1 MHz) but exhibits a more rapid cavitation propagation-growth-collapse cycle, induce comparable dissolution enhancement values  $(\sim 35\times)$  for Mg release from dolomite, due to the lower bond energy of Mg-O bonds when compared to other bonds such as Ca-O and Si-O. Although megasonic cavitation causes a significant increase in the dissolution rate of calcite (40×), ultrasonic cavitation causes an even greater increase  $(70\times)$  due to more of the higher-energy ultrasonic cavitation events meeting the threshold for the rupture of higher-bond energy Ca–O bonds. For Si-rich species which possess high bond energies, use of a megasonic frequency at a solute particle size such that the stimulation frequency corresponding to the resonance frequency of the particles provided a greater dissolution enhancement as compared to ultrasonic stimulation. Acoustic stimulation was also able to facilitate Si release from amorphous class F FA by causing ruptures in the hollow aluminosilicate FA particles.

The stacking fault energy, or energy required to induce dislocation or pit formation in a species, showed a strong correlation with both the ultrasonic and megasonic dissolution enhancement. The effectiveness of ultrasonic stimulation increased exponentially as the stacking fault energy decreased, approaching an infinite enhancement asymptote as stacking fault energy approached zero and approaching an asymptotic value of one (i.e., no enhancement) as the stacking fault energy increased. Contrarily, the effectiveness of megasonic dissolution increased linearly with the stacking fault energy, with the xintercept (1 J/m<sup>2</sup> at 1 MHz stimulation) indicating a threshold value below which megasonic cavitation events were sufficiently energetic to induce dislocations and significantly outweigh the dissolution enhancement effects of resonance vibration. The effect of resonance dissolution was further compared to the ductility (i.e., as estimated using the indentation modulus-tohardness ratio; M<sub>I</sub>/H) of materials, showing an increased effect of resonance stimulation as the ductility decreased (i.e., brittleness increased). The effect of resonance stimulation on the dissolution rate was negligible above  $M_I/H \sim 38$ . This indicates that cavitation is able to induce surface defects that facilitate dissolution in solutes with low stacking fault energies, whereas solutes with high stacking fault energies but high brittleness are more susceptible to dissolution enhancement by rapid vibration at the resonance frequency. As such, the frequency of acoustic stimulation can be appropriately matched to the intrinsic properties such as stacking fault energy and ductility of the solute(s) of interest, allowing for the use of acoustic perturbation as a green technology for the accelerated release of elements such as Si, Ca, and Mg from minerals and industrial waste materials.

# AUTHOR INFORMATION

## **Corresponding Authors**

Mathieu Bauchy — Institute for Carbon Management (ICM) and Physics of AmoRphous and Inorganic Solids Laboratory (PARISlab), Department of Civil and Environmental Engineering, University of California, Los Angeles, California 90095, United States; orcid.org/0000-0003-4600-0631; Email: bauchy@g.ucla.edu

Dante Simonetti — Institute for Carbon Management (ICM) and Department of Chemical and Biomolecular Engineering, University of California, Los Angeles, California 90095, United States; orcid.org/0000-0002-5708-460X; Email: dasimonetti@ucla.edu

Gaurav N. Sant — Laboratory for the Chemistry of Construction Materials (LC<sup>2</sup>), Department of Civil and Environmental Engineering, Institute for Carbon Management (ICM), Department of Materials Science and Engineering, and California Nanosystems Institute (CNSI), University of California, Los Angeles, California 90095, United States;

orcid.org/0000-0002-1124-5498; Email: gsant@ucla.edu

#### **Authors**

- Ross A. Arnold Laboratory for the Chemistry of Construction Materials (LC<sup>2</sup>), Department of Civil and Environmental Engineering and Institute for Carbon Management (ICM), University of California, Los Angeles, California 90095, United States; orcid.org/0000-0001-6863-8674
- Shiqi Dong Laboratory for the Chemistry of Construction Materials (LC<sup>2</sup>), Department of Civil and Environmental Engineering, Institute for Carbon Management (ICM), and Department of Materials Science and Engineering, University of California, Los Angeles, California 90095, United States
- Longwen Tang Physics of AmoRphous and Inorganic Solids Laboratory (PARISlab), Department of Civil and Environmental Engineering, University of California, Los Angeles, California 90095, United States
- Dale Prentice Laboratory for the Chemistry of Construction Materials (LC<sup>2</sup>), Department of Civil and Environmental Engineering and Institute for Carbon Management (ICM), University of California, Los Angeles, California 90095, United States
- Marie Collin Laboratory for the Chemistry of Construction Materials (LC<sup>2</sup>), Department of Civil and Environmental Engineering and Institute for Carbon Management (ICM), University of California, Los Angeles, California 90095, United States; Occid.org/0000-0002-0571-5019
- Juan Carlos Vega-Vila Institute for Carbon Management (ICM) and Department of Chemical and Biomolecular Engineering, University of California, Los Angeles, California 90095, United States
- Amaya Hernandez Department of Civil and Environmental Engineering, University of California, Los Angeles, California 90095, United States
- Erika Callagon La Plante Department of Materials Science and Engineering, University of Texas at Arlington, Arlington, Texas 76019, United States; orcid.org/0000-0002-5273-9523
- Kirk Ellison Electric Power Research Institute (EPRI), Charlotte, North Carolina 28262, United States
- Aditya Kumar Department of Materials Science and Engineering, Missouri University of Science and Technology, Rolla, Missouri 65409, United States; occid.org/0000-0001-7550-8034
- Samanvaya Srivastava Institute for Carbon Management (ICM) and Department of Chemical and Biomolecular Engineering, University of California, Los Angeles, California 90095, United States; orcid.org/0000-0002-3519-7224

Complete contact information is available at: https://pubs.acs.org/10.1021/acs.jpcc.1c10968

#### Notes

The authors declare no competing financial interest.

#### ACKNOWLEDGMENTS

The authors acknowledge financial support for this research provisioned by Department of Energy's Advanced Research Projects Agency for Energy (ARPA-E: award number: DE-AR0001147), the U.S. National Science Foundation (DMREF-1922167), and the Electric Power Research Institute (EPRI). The authors acknowledge PCT Systems Inc. for provision of a bespoke megasonic stimulation unit to the Laboratory for the Chemistry of Construction materials (LC<sup>2</sup>). In addition, Dr. Joseph King (ARPA-E) and Prof. Seth Putterman (UCLA) are

acknowledged for their insights and suggestions as related to acoustic stimulation of mineral dissolution reactions and bubble cavitation processes.

#### REFERENCES

- (1) Said, A.; Mattila, O.; Eloneva, S.; Järvinen, M. Enhancement of Calcium Dissolution from Steel Slag by Ultrasound. *Chem. Eng. Process. Process Intensif.* **2015**, 89, 1–8.
- (2) Wei, Z.; Hsiao, Y.-H.; Chen, X.; La Plante, E. C.; Mehdipour, I.; Simonetti, D.; Neithalath, N.; Pilon, L.; Bauchy, M.; Israelachvili, J.; et al. Isothermal Stimulation of Mineral Dissolution Processes by Acoustic Perturbation. *J. Phys. Chem. C* **2018**, *122*, 28665–28673.
- (3) Deb Barma, S.; R, S.; Baskey, P. K.; Biswal, S. K. Chemical Beneficiation of High-Ash Indian Noncoking Coal by Alkali Leaching under Low-Frequency Ultrasonication. *Energy Fuels* **2018**, 32, 1309—1319
- (4) Tang, X.; Liu, M.; Tang, Q.; Du, Z.; Bai, S.; Zhu, Y. Effect of Ultrasound on the Dissolution of Magnesium Hydroxide: PH-Stat and Nanoscale Observation. *Ultrason. Sonochem.* **2019**, *55*, 223–231.
- (5) Feng, D.; Aldrich, C. Effect of Ultrasonication on the Flotation of Talc. *Ind. Eng. Chem. Res.* **2004**, 43, 4422–4427.
- (6) Zhao, Q.; Liu, C.-j.; Jiang, M.-f.; Saxén, H.; Zevenhoven, R. Preparation of Magnesium Hydroxide from Serpentinite by Sulfuric Acid Leaching for CO2 Mineral Carbonation. *Miner. Eng.* **2015**, *79*, 116–124.
- (7) Ma, J.; Zhang, Y.; Qin, Y.; Wu, Z.; Wang, T.; Wang, C. The Leaching Kinetics of K-Feldspar in Sulfuric Acid with the Aid of Ultrasound. *Ultrason. Sonochem.* **2017**, *35*, 304–312.
- (8) Zhang, Y.-F.; Ma, J.; Qin, Y.-H.; Zhou, J.-F.; Yang, L.; Wu, Z.-K.; Wang, T.-L.; Wang, W.-G.; Wang, C.-W. Ultrasound-Assisted Leaching of Potassium from Phosphorus-Potassium Associated Ore. *Hydrometallurgy* **2016**, *166*, 237–242.
- (9) Balakrishnan, S.; Reddy, V. M.; Nagarajan, R. Ultrasonic Coal Washing to Leach Alkali Elements from Coals. *Ultrason. Sonochem.* **2015**, *27*, 235–240.
- (10) El[idot]k, A. i. l.; Akçay, M.; Sökmen, M. Ultrasonic Leaching of Bio-Collectors for Heavy Metal Analysis. *Int. J. Environ. Anal. Chem.* **2000**, 77, 133–145.
- (11) Dong, S.; Arnold, R.; Yang, K.; La Plante, E. C.; Bustillos, S.; Kumar, A.; Wang, B.; Balonis, M.; Neithalath, N.; Ellison, K.; et al. Rapid Elemental Extraction from Ordered and Disordered Solutes by Acoustically-Stimulated Dissolution. ACS Eng. Au 2021, 1, 122.
- (12) Oza, R.; Shah, N.; Patel, S. Recovery of Nickel from Spent Catalysts Using Ultrasonication-Assisted Leaching. *J. Chem. Technol. Biotechnol.* **2011**, 86, 1276–1281.
- (13) Didenko, Y. T.; McNamara, W. B.; Suslick, K. S. Hot Spot Conditions during Cavitation in Water. J. Am. Chem. Soc. 1999, 121, 5817–5818.
- (14) Sillanpää, M.; Pham, T.-D.; Shrestha, R. A. Ultrasound Technology in Green Chemistry. SpringerBriefs in Green Chemistry for Sustainability; Springer Netherlands, 2011.
- (15) Brennen, C. E. Cavitation and Bubble Dynamics; Cambridge University Press: Cambridge, 2013.
- (16) Apfel, R. E. Sonic Effervescence: A Tutorial on Acoustic Cavitation. In *Sonochemistry and Sonoluminescence*; Crum, L. A., Mason, T. J., Reisse, J. L., Suslick, K. S., Eds.; NATO ASI Series; Springer Netherlands: Dordrecht, 1999; pp 1–24.
- (17) Ajmal, M.; Fieg, G.; Keil, F. Analysis of Process Intensification in Enzyme Catalyzed Reactions Using Ultrasound. *Chem. Eng. Process. Process Intensif.* **2016**, *110*, 106–113.
- (18) Chu, C.-L.; Lu, T.-Y.; Fuh, Y.-K. The Suitability of Ultrasonic and Megasonic Cleaning of Nanoscale Patterns in Ammonia Hydroxide Solutions for Particle Removal and Feature Damage. *Semicond. Sci. Technol.* **2020**, *35*, 045001.
- (19) Del Campo, F. J.; Coles, B. A.; Marken, F.; Compton, R. G.; Cordemans, E. High-Frequency Sonoelectrochemical Processes: Mass Transport, Thermal and Surface Effects Induced by Cavitation in a 500 KHz Reactor. *Ultrason. Sonochem.* 1999, 6, 189–197.

- (20) Park, A.-H. A.; Fan, L.-S. CO2 Mineral Sequestration: Physically Activated Dissolution of Serpentine and PH Swing Process. *Chem. Eng. Sci.* **2004**, *59*, 5241–5247.
- (21) Okur, H.; Tekin, T.; Ozer, A. K.; Bayramoglu, M. Effect of Ultrasound on the Dissolution of Colemanite in H2SO4. *Hydrometallurgy* **2002**, *67*, 79–86.
- (22) Carletti, C.; De Blasio, C.; Miceli, M.; Pirone, R.; Westerlund, T. Ultrasonic Enhanced Limestone Dissolution: Experimental and Mathematical Modeling. *Chem. Eng. Process. Process Intensif.* **2017**, 118, 26–36.
- (23) Jiao, L.; Tong, Y.; Cui, Y.; Chen, J.; Bai, Q. Research on Ultrasonic Cleaning Technology of Optical Components. 7th International Symposium on Advanced Optical Manufacturing and Testing Technologies: Advanced Optical Manufacturing Technologies; International Society for Optics and Photonics, 2014; Vol. 9281, p 928112.
- (24) Busnaina, A. A.; Kashkoush, I. I.; Gale, G. W. An Experimental Study of Megasonic Cleaning of Silicon Wafers. *J. Electrochem. Soc.* 1995, 142, 2812.
- (25) Gale, G. W.; Busnaina, A. A. Removal of Particulate Contaminants Using Ultrasonics and Megasonics: A Review. *Part. Sci. Technol.* **1995**, *13*, 197–211.
- (26) Kuyel, B. Single Wafer Megasonic Cleaner Method, System, and Apparatus. U.S. Patent 6,730,176 B2, May 4, 2004.
- (27) Loxley, T. A. Wafer Cleaning System. U.S. Patent 7,674,695 B1, March 9, 2010.
- (28) Busnaina, A. Fast Single-Article Megasonic Cleaning Process for Single-Sided or Dual-Sided Cleaning. U.S. Patent 20,010,013,355 A1, August 16, 2001.
- (29) Kim, H.; Lee, Y.; Lim, E. Development of Cooling Technology in a Megasonic Cleaning System for Flat Panel Display. *Proceeding of First Thermal and Fluids Engineering Summer Conference*; Begellhouse: New York, USA, 2016.
- (30) Shende, H.; Singh, S.; Baugh, J.; Mann, R.; Dietze, U.; Dress, P. Megasonic Cleaning: Possible Solutions for 22nm Node and Beyond. *Photomask Technology* 2011; International Society for Optics and Photonics, 2011; Vol. 8166, p. 816614.
- (31) Helbig, S.; Urban, S.; Klein, E.; Singh, S. Impact of MegaSonic Process Conditions on PRE and Sub-Resolution Assist Feature Damage. *Photomask Technology*, 2008; International Society for Optics and Photonics, 2008; Vol. 7122, p 712210.
- (32) Brennen, C. E. Cavitation and Bubble Dynamics; Cambridge University Press, 2014.
- (33) Gale, G. W.; Busnaina, A. A. Roles of Cavitation and Acoustic Streaming in Megasonic Cleaning. *Part. Sci. Technol.* **1999**, *17*, 229–238.
- (34) Church, C. C. Spontaneous Homogeneous Nucleation, Inertial Cavitation and the Safety of Diagnostic Ultrasound. *Ultrasound Med. Biol.* **2002**, *28*, 1349–1364.
- (35) Hynynen, K. The Threshold for Thermally Significant Cavitation in Dog's Thigh Muscle in Vivo. *Ultrasound Med. Biol.* **1991**, *17*, 157–169.
- (36) Crum, L. A. Bjerknes Forces on Bubbles in a Stationary Sound Field. J. Acoust. Soc. Am. 1975, 57, 1363–1370.
- (37) Leighton, T. G.; Walton, A. J.; Pickworth, M. J. W. Primary Bjerknes Forces. Eur. J. Phys. 1990, 11, 47–50.
- (38) Kang, B.-K.; Kim, M.-S.; Park, J.-G. Effect of Dissolved Gases in Water on Acoustic Cavitation and Bubble Growth Rate in 0.83MHz Megasonic of Interest to Wafer Cleaning. *Ultrason. Sonochem.* **2014**, 21, 1496–1503.
- (39) Luo, Y.-R. Bond Dissociation Energies. *CRC Handbook of Chemistry and Physics*, 89th ed.; CRC Press/Taylor and Francis, 2009; pp 66–70.
- (40) Tang, L.; Dong, S.; Arnold, R.; La Plante, E. C.; Vega-Vila, J. C.; Prentice, D.; Ellison, K.; Kumar, A.; Neithalath, N.; Simonetti, D.; et al. Atomic Dislocations and Bond Rupture Govern Dissolution Enhancement under Acoustic Stimulation. *ACS Appl. Mater. Interfaces* **2020**, *12*, 55399.

- (41) Rusinko, A. Influence of Preliminary Ultrasonic Treatment upon the Steady-State Creep of Metals of Different Stacking Fault Energies. *Ultrasonics* **2014**, *54*, 90–98.
- (42) Zhang, X.-F.; Fang, L. The Effect of Stacking Fault Energy on the Cavitation Erosion Resistance of  $\alpha$ -Phase Aluminum Bronzes. *Wear* **2002**, 253, 1105–1110.
- (43) Richman, R. H.; McNaughton, W. P. Correlation of Cavitation Erosion Behavior with Mechanical Properties of Metals. *Wear* **1990**, 140, 63–82.
- (44) Romdhane, M.; Gourdon, C. Investigation in Solid-Liquid Extraction: Influence of Ultrasound. *Chem. Eng. J.* **2002**, *87*, 11–19.
- (45) Fei, C.; Chiu, C. T.; Chen, X.; Chen, Z.; Ma, J.; Zhu, B.; Shung, K. K.; Zhou, Q. Ultrahigh Frequency (100 MHz–300 MHz) Ultrasonic Transducers for Optical Resolution Medical Imagining. *Sci. Rep.* **2016**, *6*, 28360.
- (46) Plimpton, S. Fast Parallel Algorithms for Short-Range Molecular Dynamics. *J. Comput. Phys.* **1995**, *117*, 1–19.
- (47) Nosé, S. A Unified Formulation of the Constant Temperature Molecular Dynamics Methods. *J. Chem. Phys.* **1984**, *81*, 511–519.
- (48) Hoover, W. G. Canonical Dynamics: Equilibrium Phase-Space Distributions. *Phys. Rev. A* 1985, 31, 1695–1697.
- (49) Yaoita, A.; Adachi, T.; Yamaji, A. Determination of Elastic Moduli for a Spherical Specimen by Resonant Ultrasound Spectroscopy. *NDT E Int.* **2005**, *38*, 554–560.
- (50) Du, J.; Cormack, A. N. The Medium Range Structure of Sodium Silicate Glasses: A Molecular Dynamics Simulation. *J. Non-Cryst. Solids* **2004**, 349, 66–79.
- (51) Maslen, E. N.; Streltsov, V. A.; Streltsova, N. R. X-Ray Study of the Electron Density in Calcite, CaCo3. *Acta Crystallogr., Sect. B: Struct. Sci.* **1993**, *49*, 636–641.
- (52) Raiteri, P.; Demichelis, R.; Gale, J. D. Thermodynamically Consistent Force Field for Molecular Dynamics Simulations of Alkaline-Earth Carbonates and Their Aqueous Speciation. *J. Phys. Chem. C* 2015, 119, 24447–24458.
- (53) Beran, A.; Zemann, J. Refinement and Comparison of the Crystal Structures of a Dolomite and of an Fe-Rich Ankerite. *Tschermaks Mineral. Petrogr. Mittl.* **1977**, 24, 279–286.
- (54) Prewitt, C. T.; Sueno, S.; Papike, J. J. The Crystal Structures of High Albite and Monalbite at High Temperatures. *Am. Mineral.* **1976**, *61*, 1213–1225.
- (55) Cygan, R. T.; Liang, J.-J.; Kalinichev, A. G. Molecular Models of Hydroxide, Oxyhydroxide, and Clay Phases and the Development of a General Force Field. *J. Phys. Chem. B* **2004**, *108*, 1255–1266.
- (56) Will, G.; Bellotto, M.; Parrish, W.; Hart, M. Crystal Structures of Quartz and Magnesium Germanate by Profile Analysis of Synchrotron-Radiation High-Resolution Powder Data. *J. Appl. Crystallogr.* **1988**, 21, 182–191.
- (57) van Beest, B. W. H.; Kramer, G. J.; van Santen, R. A. Force Fields for Silicas and Aluminophosphates Based on Ab Initio Calculations. *Phys. Rev. Lett.* **1990**, *64*, 1955–1958.
- (58) Rice, J. R.; Thomson, R. Ductile versus Brittle Behaviour of Crystals. *Philos Mag J Theor Exp Appl Phys* **1974**, 29, 73–97.
- (59) Wei, Z.; Villamena, F. A.; Weavers, L. K. Kinetics and Mechanism of Ultrasonic Activation of Persulfate: An in Situ EPR Spin Trapping Study. *Environ. Sci. Technol.* **2017**, *51*, 3410–3417.
- (60) Luce, R. W.; Bartlett, R. W.; Parks, G. A. Dissolution Kinetics of Magnesium Silicates. *Geochim. Cosmochim. Acta* **1972**, *36*, 35–50.
- (61) Busenberg, E.; Clemency, C. V. The Dissolution Kinetics of Feldspars at 25°C and 1 Atm CO2 Partial Pressure. *Geochim. Cosmochim. Acta* 1976, 40, 41–49.
- (62) Holdren, G. R.; Adams, J. E. Parabolic Dissolution Kinetics of Silicate Minerals: An Artifact of Nonequilibrium Precipitation Processes? *Geology* **1982**, *10*, 186–190.
- (63) George, J. L.; Brow, R. K. In-Situ Characterization of Borate Glass Dissolution Kinetics by  $\mu$ -Raman Spectroscopy. *J. Non-Cryst. Solids* **2015**, 426, 116–124.
- (64) Suslick, K. S. Sonochemistry. Science 1990, 247, 1439-1445.
- (65) Brotchie, A.; Borisova, D.; Belova, V.; Möhwald, H.; Shchukin, D. Ultrasonic Modification of Aluminum Surfaces: Comparison between

Thermal and Ultrasonic Effects. J. Phys. Chem. C 2012, 116, 7952-7956.

- (66) Radziuk, D.; Möhwald, H.; Shchukin, D. Ultrasonic Activation of Platinum Catalysts. *J. Phys. Chem. C* **2008**, *112*, 19257–19262.
- (67) Sandlöbes, S.; Friák, M.; Zaefferer, S.; Dick, A.; Yi, S.; Letzig, D.; Pei, Z.; Zhu, L.-F.; Neugebauer, J.; Raabe, D. The Relation between Ductility and Stacking Fault Energies in Mg and Mg—Y Alloys. *Acta Mater.* **2012**, *60*, 3011–3021.
- (68) Sun, P.-L.; Zhao, Y. H.; Cooley, J. C.; Kassner, M. E.; Horita, Z.; Langdon, T. G.; Lavernia, E. J.; Zhu, Y. T. Effect of Stacking Fault Energy on Strength and Ductility of Nanostructured Alloys: An Evaluation with Minimum Solution Hardening. *Mater. Sci. Eng., A* **2009**, 525, 83–86.
- (69) Tian, Y.; Shibata, A.; Zhang, Z.; Tsuji, N. Ductility Sensitivity to Stacking Fault Energy and Grain Size in Cu—Al Alloys. *Mater. Res. Lett.* **2016**, *4*, 112—117.
- (70) Zhao, Y. H.; Zhu, Y. T.; Liao, X. Z.; Horita, Z.; Langdon, T. G. Tailoring Stacking Fault Energy for High Ductility and High Strength in Ultrafine Grained Cu and Its Alloy. *Appl. Phys. Lett.* **2006**, *89*, 121906.
- (71) Kazembeyki, M.; Bauchy, M.; Hoover, C. G. New Insights into the Indentation Size Effect in Silicate Glasses. *J. Non-Cryst. Solids* **2019**, 521, 119494.
- (72) Constantinides, G.; Ulm, F.-J. The Nanogranular Nature of C-S-H. *J. Mech. Phys. Solid.* **2007**, *SS*, 64–90.
- (73) Hoover, C. G.; Ulm, F.-J. Experimental Chemo-Mechanics of Early-Age Fracture Properties of Cement Paste. *Cem. Concr. Res.* **2015**, 75, 42–52.
- (74) Abdolhosseini Qomi, M. J.; Krakowiak, K. J.; Bauchy, M.; Stewart, K. L.; Shahsavari, R.; Jagannathan, D.; Brommer, D. B.; Baronnet, A.; Buehler, M. J.; Yip, S.; Ulm, F.-J.; Van Vliet, K. J.; Pellenq, R. J. M. Combinatorial Molecular Optimization of Cement Hydrates. *Nat. Commun.* **2014**, *5*, 4960.
- (75) Berthonneau, J.; Hoover, C. G.; Grauby, O.; Baronnet, A.; Pellenq, R. J.-M.; Ulm, F.-J. Crystal-Chemistry Control of the Mechanical Properties of 2:1 Clay Minerals. *Appl. Clay Sci.* **2017**, 143, 387–398.

# ☐ Recommended by ACS

# Rapid Elemental Extraction from Ordered and Disordered Solutes by Acoustically-Stimulated Dissolution

Shiqi Dong, Gaurav Sant, et al.

SEPTEMBER 07, 2021

ACS ENGINEERING AU

READ 🗹

#### Impact of Hydrodynamic and Interfacial Interactions on Scale Formation in a Capillary Microchannel

Amir Hossein Nikoo and Mohammad Reza Malayeri

NOVEMBER 11, 2021

LANGMUIR

READ 🗹

## Acid Erosion of Carbonate Fractures and Accessibility of Arsenic-Bearing Minerals: *In Operando* Synchrotron-Based Microfluidic Experiment

Hang Deng, Catherine A. Peters, et al.

AUGUST 26, 2020

ENVIRONMENTAL SCIENCE & TECHNOLOGY

READ [7]

#### Dissolution of Minerals Driven by the Wetting Film in Rock Pores: Comparison of Silicates and Carbonates

Tadashi Yokoyama and Naoki Nishiyama

NOVEMBER 01, 2020

ACS EARTH AND SPACE CHEMISTRY

READ 🗹

Get More Suggestions >